ORIGINAL ARTICLE

Journal
of the American Ceramic Society

Ionic occupation, structures, and microwave dielectric properties of Y$_3$MgAl$_3$SiO$_{12}$ garnet-type ceramics

Jianbing Song[1] | **Kaixin Song**[1] (iD) | **Jinsheng Wei**[1] | **Huixin Lin**[2] | **Jun Wu**[1] | **Junming Xu**[1] | **Weitao Su**[3] | **Zhiqun Cheng**[1]

[1]College of Electronic Information and Engineering, Hangzhou Dianzi University, Hangzhou, China

[2]Shanghai Institute of Ceramics, Chinese Academy of Sciences, Shanghai, China

[3]College of Materials Sciences and Environmental Engineering, Hangzhou Dianzi University, Hangzhou, China

Correspondence
Kaixin Song, College of Electronic Information and Engineering, Hangzhou Dianzi University, Hangzhou, China.
Email: kxsong@hdu.edu.cn

Abstract
The Y$_3$MgAl$_3$SiO$_{12}$ ceramics with pure phase were successfully synthesized by solid-state sintering reaction method for the first time. Their microwave dielectric properties were investigated as a function of sintering temperature. Their microstructure characteristics and ionic occupation sites of tetrahedral and octahedral units were characterized and analyzed by SEM& energy dispersive spectrometer (EDS) and Rietveld refinement of X-ray powder diffraction data. Crystal structure of Y$_3$MgAl$_3$SiO$_{12}$ is isostructural to Y$_3$Al$_5$O$_{12}$ with a cubic garnet structure and space group of Ia-3d, which contains YO$_8$ dodecahedra, (Mg/Al$_{oct}$)O$_6$ octahedral, and (Si/Al$_{tet}$)O$_4$ tetrahedral units. The Qf and ε$_r$ values of different samples are strongly dependent on the distribution of grain sizes, grain sizes, and porosity. The samples sintered at 1550°C exhibit optimized microwave dielectric properties with relative permittivity (ε$_r$) of 10.1, Qf values of 57 340GHz (at 9.5 GHz), and τ$_f$ values of −32 ppm/°C. Such properties indicate potential application of Y$_3$MgAl$_3$SiO$_{12}$ as microwave substrates.

KEYWORDS
dielectric materials/properties, electroceramics, microstructure, yttrium aluminum garnet

1 | INTRODUCTION

With the rapid growth of the Information Communications Technology (ICT) involving Wi-Fi gadgets, mobile devices, satellite communication systems and radar technology, considerable researches had been focused on microwave dielectric ceramics.[1,2] Up to now, many materials with high quality factor (Qf values) to depress energy loss, low dielectric constant (ε$_r$) to reduce the delay time of electronic signal transmission, and ideal near zero temperature coefficient of resonant frequency (τ$_f$) for working frequency stability have been reported and used as resonators, filters, dielectric antennas, dielectric guided wave circuits, and other microwave components.[3] However, the demand for research and development of new dielectric materials with excellent

behaviors is not keeping up with the advancement steps of ICT.[4]

To solve these problems, various kinds of silicate ceramic materials, such as forsterite Mg$_2$SiO$_4$,[5] willemite Zn$_2$SiO$_4$,[6] Al$_2$SiO$_5$,[7] cordierite Mg$_2$Al$_4$Si$_5$O$_{18}$,[8] Sr$_2$Al$_2$SiO$_7$,[9] etc., had been fabricated to act as microwave and millimeter wave devices in recent years. Due to strong effects of covalent bond in silicate basic units of [SiO$_4$] tetrahedrons, silicates usually have low dielectric constants.[10] However, unfortunately their dielectrics loss (tanδ) or temperature stability is not good enough to act as desirable dielectrics. Although high Qf values more than 200 000 GHz were reported for Mg$_2$SiO$_4$, Zn$_2$SiO$_4$, and Mg$_2$Al$_4$Si$_5$O$_{18}$,[5,6,8] it is very difficult to tune negative temperature coefficients of resonant frequency of these materials to be zero by solid solution modification or addition of universal positive

temperature coefficients materials. Recently some new silicate ceramics with better microwave properties and microstructures were continuingly investigated. For example, the microwave dielectric properties of $Ba_2ZnSi_2O_7$ were reported by Lei et al with ferroelectric characteristics at temperature higher than 500°C.[11] Sebastian et al reported sillimanite (Al_2SiO_5) has low $\varepsilon_r = 4.4$, $Qf = 41\ 800$ GHz with $\tau_f = -17$ ppm/°C.[7] Regarding to these initial progresses of silicate dielectrics, there still remain broad spaces to develop novel compounds and explore their microwave dielectric characteristics.

Rare earth aluminum garnets like $Y_3Al_5O_{12}$ have cubic garnet structure with a general formula $X_3Y_2Z_3O_{12}$, in which atoms X, Y, and Z occupy the lattice sites of 24c, 16a, and 24d, respectively.[12] Previously theoretical studies had been usually focused on the physical properties and luminous characteristics of the rare earth doped and undoped garnet crystals and powders. Papagelis, et al reported lattice dynamical properties of the Rare Earth Aluminum Garnets.[13] Zorenko, et al studied photoluminescence properties of new garnet structure phosphors.[14] In this article, we initially report the novel microwave dielectric properties of $Y_3MgAl_3SiO_{12}$ ceramics, which belongs to one kind of aluminum garnet family. Crystal structure parameters of the ceramic powder were refined via the Rietveld method of X-ray diffraction (XRD). The crystal structure of $Y_3MgAl_3SiO_{12}$ can be seen as the Mg^{2+}–Si^{4+}ionic pairs substitute for the Al^{3+}–Al^{3+}ionic pairs, which can also be regarded as chemical units of $[MgO_6]$/$[SiO_4]$ replacing $[AlO_6]$/$[AlO_4]$ polyhedral. Mg/Si possible ionic occupation sites, the dependence of grain sizes, distribution of grain sizes, and porosity on microwave dielectric properties are discussed in the paper.

2 | EXPERIMENTAL PROCEDURE

High-density samples were fabricated by a conventional solid-state sintering method using high-purity powders Y_2O_3 (Aladdin Industrial Corporation, 99.9%), MgO (Sinopharm Chemical ReagentCo., Ltd, 99.9%), SiO_2 (Sinopharm Chemical ReagentCo., Ltd, 99.99%), Al_2O_3 (Sinopharm Chemical ReagentCo., Ltd, 99.99%) as raw materials. Firstly, MgO powders were calcinated at 1000°C for 3 hours to remove water and CO_2 due to its hygroscopic. Stoichiometric proportions of above powders were weighted according to chemical formula of $Y_3MgAl_3SiO_{12}$ and mixed in ethanol for 24 hours with zirconia balls as milling media. The obtained slurries were dried and then calcined at 1350°C for 4 hours. After ball re-milled, the calcined powders were mixed with 5 wt% solution of polyvinyl alcohol and pressed into pellets at the pressure of 100 MPa using a stainless die. Then, the pellets were sintered at 1400°C to 1600°C and cooled to 1000°C and then shut down the power, further cooled inside the furnace to room temperature.

The bulk density of the sintered pellets was measured by the Archimedes method using distilled water as medium. The room-temperature crystalline phase constituents were identified by XRD (RIGAKU D/max 2550/PC, Rigaku Co., Tokyo, Japan) using Cu K radiation ($\lambda = 1.54056$ Å) radiation at the voltage of 40 kV and current of 30 mA. The scanning rate was 10° min^{-1} in the 2θ range from 10° to 90°. The data for the Rietveld analysis were collected in a step-scanning mode with a step size of 0.02° and 5 seconds counting time per step over a 2θ range from 5° to 120°. The Rietveld refinement on the XRD patterns was carried out using the general structure analysis system (GSAS) software.[15] The surface morphology of the polished and thermal etched samples was observed using Field Emission Scanning Electron Microscopy (Ultra55, Germany) equipped with an energy dispersive spectrometer (EDS). The dielectric constant (ε_r) and quality values (Qf) were determined by the paralleling plate method[16] using a vector network analyzer (E8363B, Agilent Technologies Inc., Santa Clara, CA). The temperature coefficient of the resonant frequency (τ_f) at 20°C to 80°C was measured using by the resonant-cavity method[17] using a silver-coated cavity connected to the network analyzer. To ensure the accuracy of the data, at least two samples were measured for each composition.

3 | RESULTS AND DISCUSSION

Figure 1 presents XRD spectra of $Y_3MgAl_3SiO_{12}$ samples sintered at different temperature. All diffraction curves are similar to each other and match well with standard $Y_3Al_5O_{12}$ sample (PDF No.33-0040). In these spectra, no secondary phases can be observed.

The crystal structure of $Y_3MgAl_3SiO_{12}$ analogs to that of $Y_3Al_5O_{12}$, its space group can also be assigned to Ia-3d. The crystal structure parameters of $Y_3MgAl_3SiO_{12}$ were further refined with the pristine structure model of $Y_3Al_5O_{12}$ based on the Rietveld method using GSAS software. The obtained lattice parameters are $a = b = c = 12.0548$Å and $\alpha = \beta = \gamma = 90°$. In the structure of $Y_3Al_5O_{12}$, Y atoms occupy 24c sites where its dodecahedral coordinated with oxygen atoms, and Al atoms are located in two different sites: Al_{oct} occupy 16a with octahedral point symmetry (S6) and Al_{tet} occupy 24d with tetrahedral point symmetry (S4). Oxygen atoms are located at 96 hours sites defined by three internal parameters x, y, z. Each oxygen atom is shared by an AlO_4 tetrahedron, an AlO_6 octahedron and two equivalent YO_8 dodecahedra.[18] The formula of $Y_3MgAl_3SiO_{12}$ might be considered as
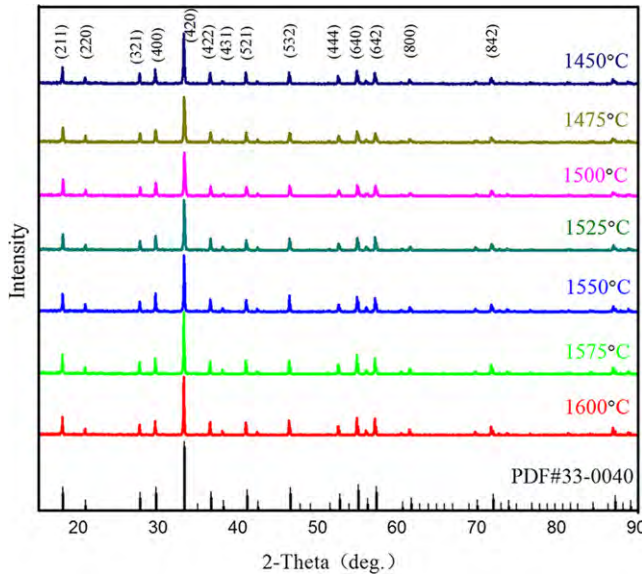
FIGURE 1 X-ray diffraction pattern of $Y_3MgAl_3SiO_{12}$ ceramic powders sintered at different temperature

$Y_3Al_3(Mg, Si)O_{12}$, where Al ions were replaced by Mg and Si ions in $Y_3Al_5O_{12}$, respectively. However, there are seven possibilities for the specific location of Mg and Si ions, such as:

(i) Mg occupy Al_{oct} and Si occupy Al_{tet}, ($Al_{oct}(Mg)Al_{tet}$ (Si)); (ii) Si occupy Al_{oct} and Mg occupy Al_{tet}, ($Al_{oct}(Si)$ $Al_{tet}(Mg)$); (iii) Mg occupy Al_{oct} and (Mg, Si) occupy Al_{tet}, ($Al_{oct}(Mg)Al_{tet}(Mg, Si)$); (iv) Si occupy Al_{oct} and (Mg, Si) occupy Al_{tet}, ($Al_{oct}(Si)Al_{tet}$ (Mg, Si)); (v) (Mg, Si) occupy Al_{oct} and Mg occupy Al_{tet}, ($Al_{oct}(Mg, Si)Al_{tet}(Mg)$); (vi) (Mg, Si) occupy Al_{oct} and Si occupy Al_{tet}, ($Al_{oct}(Mg, Si)$ Al_{tet} (Si)); (vii) (Mg, Si) occupy Al_{oct} and (Mg, Si) occupy Al_{tet}, ($Al_{oct}(Mg, Si)Al_{tet}$ (Mg, Si)).

The most possible atomic occupation position can be obtained by Rietveld method based on GSAS software. The fitting qualities of the experimental data have been assessed by computing the fitting parameters such as the "goodness of fit" $\chi2$, and various R-factors such as Rp (profile factor), R_{wp} (weighted profile factor), R_{exp} (expected weighted profile factor) which are defined as following[19]

$$Profile\ factor, R_p = 100 \frac{\sum_{i=1,n} |y_i - y_{c,i}|}{\sum_{i=1,n} y_i} \quad (1)$$

Where, "y_i" is the observed point (experimental) and "$y_{c,i}$" is the calculated point and n represents the number of data points.

$$Weighted\ profile\ factor, R_{wp} = 100 \left[\frac{\sum_{i=1,n} \omega_i |y_i - y_{c,i}|^2}{\sum_{i=1,n} \omega_i y_i^2} \right]^{1/2}$$
$$(2)$$

Where, $\omega_i = \frac{1}{\sigma^2}$, σ^2 is the variance of observation y_i.

$$Expected\ weight\ factor, R_{exp} = 100 \left[\frac{n-p}{\sum_{i=1,n} \omega_i y_i^2} \right]^{1/2} \quad (3)$$

Here, $(n–p)$ is the number of degrees of freedom. "n" is the total number of experimental points and "p" is the number of refined parameters.

Reduced chi-square, $\chi^2 = \left[\frac{R_{wp}}{R_{exp}} \right]^2$, the low value of χ^2 (goodness of fit) justifies the goodness of refinement.

Table 1 gives the Refined parameters for seven possible ionic occupation operated by GASA software. The optimal quality value of R_{wp}, R_p, and χ^2 were 6.73%, 4.73%, and 2.6, respectively, which confirming that the first assumption of $Al_{oct}(Mg)Al_{tet}(Si)$ is the most possible and appropriate than other assumptions. The obtained unit cell volume, $V = 1751.77$ Å^3, corresponds to an equilibrium cubic crystal lattice constant of 12.0548 Å^3.

As shown in Figure 2, the calculated values of $Al_{oct}(Mg)Al_{tet}(Si)$ ionic occupation agree well with the experimental results, which indicates the ionic occupations obtained by Refined method are rational. Table 2 summarizes the optimally refined structural parameters and each atomic position. It can be seen that Mg and Si ions have the same coordinate sites with the Al_{oct} and Al_{tet}, respectively.

As seen the insert figure of Figure 2, the cubic crystal structure of $Y_3MgAl_3SiO_{12}$ is composed of $Al/Si–O_4$ tetrahedron, $Al/Mg–O_6$ octahedral and $Y–O_8$ dodecahedra. The YO_8 dodecahedrons are connected together with $(Al/Mg)O_6$ octahedrons by their shared edges and with $(Al/Si)O_4$ dodecahedrons by O atom and edges. Every YO_8 dodecahedron is surrounded by four YO_8 dodecahedron, four $(Al/Si)O_6$ octahedrons and six $(Al/Si)O_4$ tetrahedrons. Each oxygen ion is shared by a tetrahedron, an octahedron and two dodecahedra. The YO_8 dodecahedra are slightly distorted with two different Y–O bond distances, $(Y–O)1 = 2.29$Å and $(Y–O)2 = 2.44$Å. While the Al_{oct}–O and Al_{tet}–O bond distances are 1.99Å and 1.74Å for $Al_{oct}O_6$ and $Al_{tet}O_4$, respectively.

TABLE 1 Refined parameters after being fitted on the different position by GASA software

$Y_3MgAl_3SiO_{12}$	R_{wp}	R_p	χ^2
$Al_{oct}(Mg)Al_{tet}(Si)$	6.37%	4.73%	2.6
$Al_{oct}(Si)Al_{tet}(Mg)$	12.8%	10.4%	6.5
$Al_{oct}(Mg)Al_{tet}(Mg,Si)$	21.2%	11.4%	15.6
$Al_{oct}(Si)Al_{tet}(Mg,Si)$	21.9%	14.8%	11.8
$Al_{oct}(Mg,Si)Al_{tet}(Mg)$	34.5%	23.3%	19.7
$Al_{oct}(Mg,Si)Al_{tet}(Si)$	19.7%	14.3%	7.2
$Al_{oct}(Mg,Si)Al_{tet}(Mg,Si)$	30.5%	20.5%	26.4
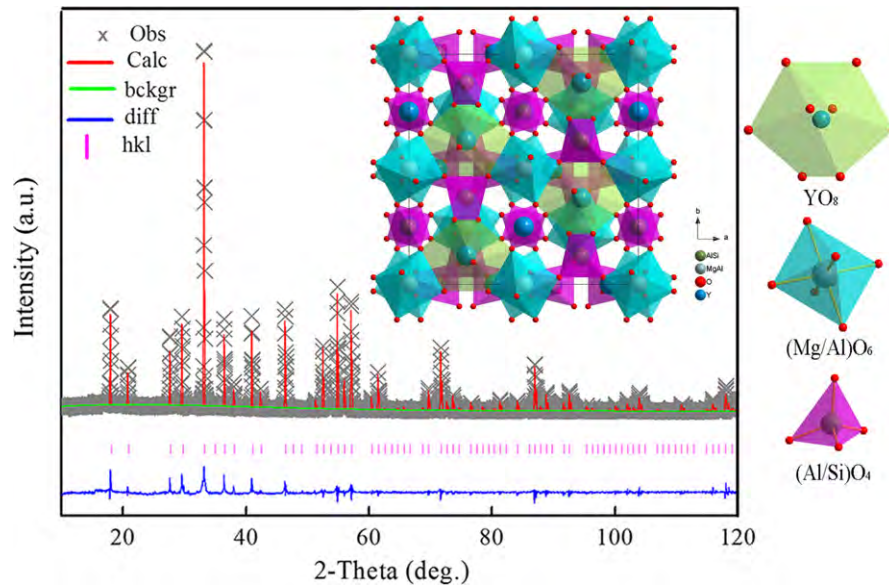
FIGURE 2 Rietveld refinement pattern and crystal structure diagram of $Y_3MgAl_3SiO_{12}$ sample sintered at 1550°C for 4 h

TABLE 2 Refined atomic positions and crystal structure parameters of $Y_3MgAl_3SiO_{12}$ ceramics by Rietveld refinement of XRD

Atom	Wyck	a	b	c	Occupancy
Y	24c	0	0.25	0.125	1.00
Al_{oct}	16a	0	0	0	0.50
Al_{tet}	24d	0	0.25	0.375	0.667
Mg	16a	0	0	0	0.50
Si	24d	0	0.25	0.375	0.333
O	96 h	−0.030473	0.051780	0.153989	1.00
Space group:	a	b	c	$\alpha = \beta = \gamma$	V
Ia-3d	12.0548Å	12.0548Å	12.0548Å	90°	1751.77 $Å^3$

Figure 3 shows the SEM images and EDS profiles of $Y_3MgAl_3SiO_{12}$ ceramics sintered at various temperatures. Figure a-c show the grain morphology of $Y_3MgAl_3SiO_{12}$ ceramics sintered at 1450°C, 1525°C, and 1550°C, respectively. It is observed that there are many holes between grains and the grain sizes of particles are small. With the augment of sintering temperature from 1550°C to 1600°C, shown in Figure c-e, the particle grain boundaries gradually become clear and distinct. Meanwhile, the grains grow up and holes disappear. The sample sintered at 1550°C exhibits a uniform grain sizes. As sintering temperature increases to 1600°C, the grains continue to grow up. However, there are no over burnt phenomenon observed on the surface of ceramics. The EDS analysis in Figure 3f detected in Figure 3d shows that the molar ratio of Y, Mg, Al, Si, and O elements are 3.4: 1: 2.7: 1.3: 9.4, which is close to molar ratio of $Y_3MgAl_3SiO_{12}$.

Figure 4 displays the approximate statistical distribution of grains sizes measured by the Image J software. The surface area of all grains was measured according to SEM image. As shown in Figure 4a, the distribution of grain sizes becomes more nonuniform as the increase in sintering temperature. Uniform distribution of grain sizes are obtained for samples sintered at 1525°C and 1550°C. Herein, the dispersion degree of distribution of grain sizes (σ) is committed to check the uniformity of distribution of grain sizes. As reference to the formula of
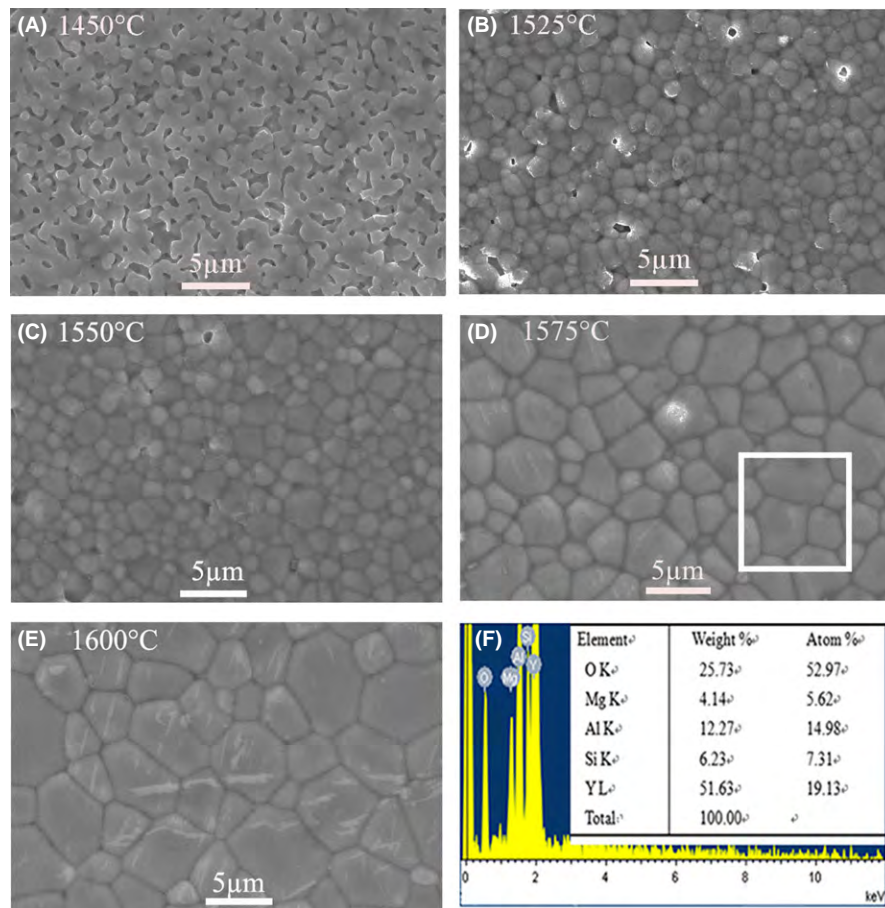
$$\overline{S} = \frac{1}{n}\sum_{i=1}^{n} S_i, \tag{5}$$

$$\sigma = \sqrt{\frac{\sum_{i=1}^{n}\left(S_i - \overline{S}\right)^2}{n}} \tag{6}$$

Where $\overline{S}$ and σ are average surface area of grain particles and dispersion degree of distribution of grain sizes, respectively.

As plotted in Figure 4b, the average grain surface area increase and the values are about 1.43 μm^2 at 1525°C,

FIGURE 3 SEM images of the $Y_3MgAl_3SiO_{12}$ ceramics: (a) 1450°C, (b) 1525°C, (c) 1550°C, (d)1575°C, (e)1600°C, and (f) energy dispersive spectrometer result for 1575°C

2.04 μm^2 at 1550°C, 3.98 μm^2 at 1575°C and 11.78 μm^2 at 1600°C, respectively. The dispersion degree (σ) becomes large with increasing sintering temperature, which illustrates that the distribution of grain sizes gradually becomes nonuniform as a function of sintering temperature.

The bulk relative densities, quality factors (Qf values), dielectric constants (ε_r), τ_f values of the sintered samples are shown in Figure 5. As shown Figure 5a, the relative densities of $Y_3MgAl_3SiO_{12}$ samples are calculated according to the followed formula:

$$\rho_{rel} = \rho_{mea} \cdot \frac{NV}{ZM} \qquad (7)$$

Where, ρ_{rel} and ρ_{mea} are the relative densities and measured densities, respectively. N is the Avogadro number and M is the molar weight. The V and Z are the volume and number of atoms of per unit cell.[20] It is easy found the density of samples gradually increases with increasing sintering temperature from 1450°C to 1600°C. No inflection point can be observed on the relative density curve, which hints the densification sintering temperature might be 1600°C or higher. The density curve matches well with the SEM pictures where

the grains are not fully grown under 1550°C and there is some porosity between particles which lead to the low relative densities. The relative densities increase continuously with the increasing grain size when the sintering temperature over 1550°C. Figure 5b shows the Qf values of the $Y_3MgAl_3SiO_{12}$ ceramics gradually increase from 16 740 GHz to 57 340 GHz as the sintering temperature increases from 1450°C to 1550°C, and then decreases slightly to 53 540 GHz when the sintering temperature at 1600°C. Generally, the quality factors (Qf values) are mainly dominated by intrinsic factors such as ionic polarization and crystalline structure, as well as extrinsic losses which arise from the presence of defects such as secondary phases, grain size, distribution of gain size, grain boundary, oxygen vacancy and porosity.[21] Except effect of secondary phases in pure $Y_3MgAl_3SiO_{12}$ ceramics, taking Figure 4 into account, it can be inferred that the grain sizes and distribution of grain sizes have a critical impact on Q_f values in our samples. Moreover, the grain sizes are appropriate to 2-4 μm for better Qf value. According to the references addressed by Wang, et al,[22] the sintered temperature, furnace cooling atmosphere, as well as the density might affect oxygen vacancy to exclude
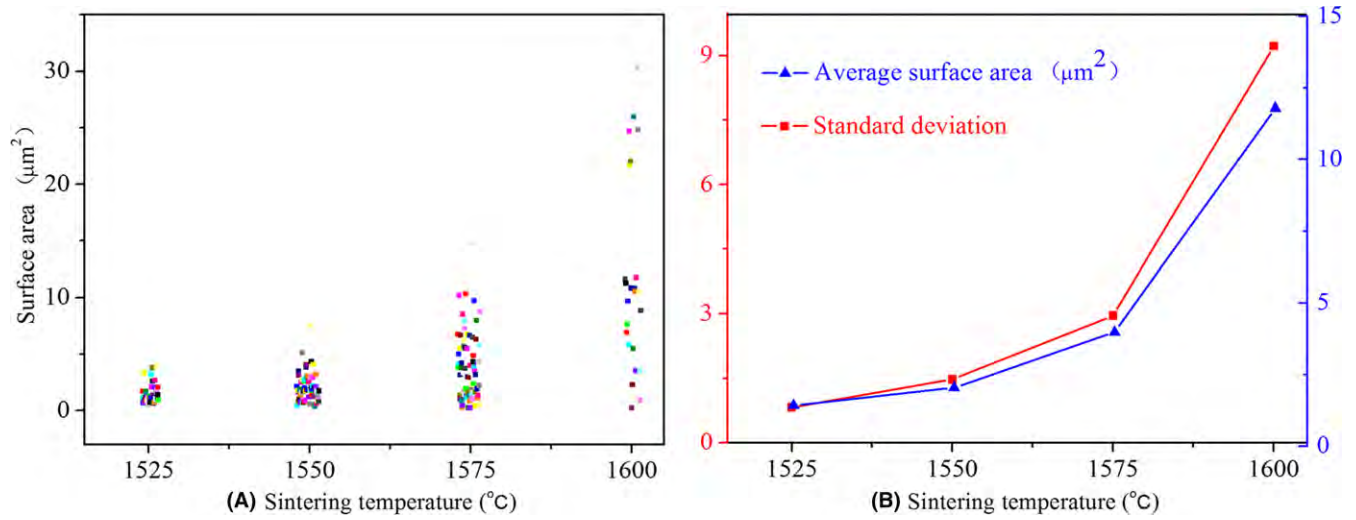
FIGURE 4 (a) the distribution of grains sizes, (b) the average surface area and dispersion degree of grain size at different sintering temperature
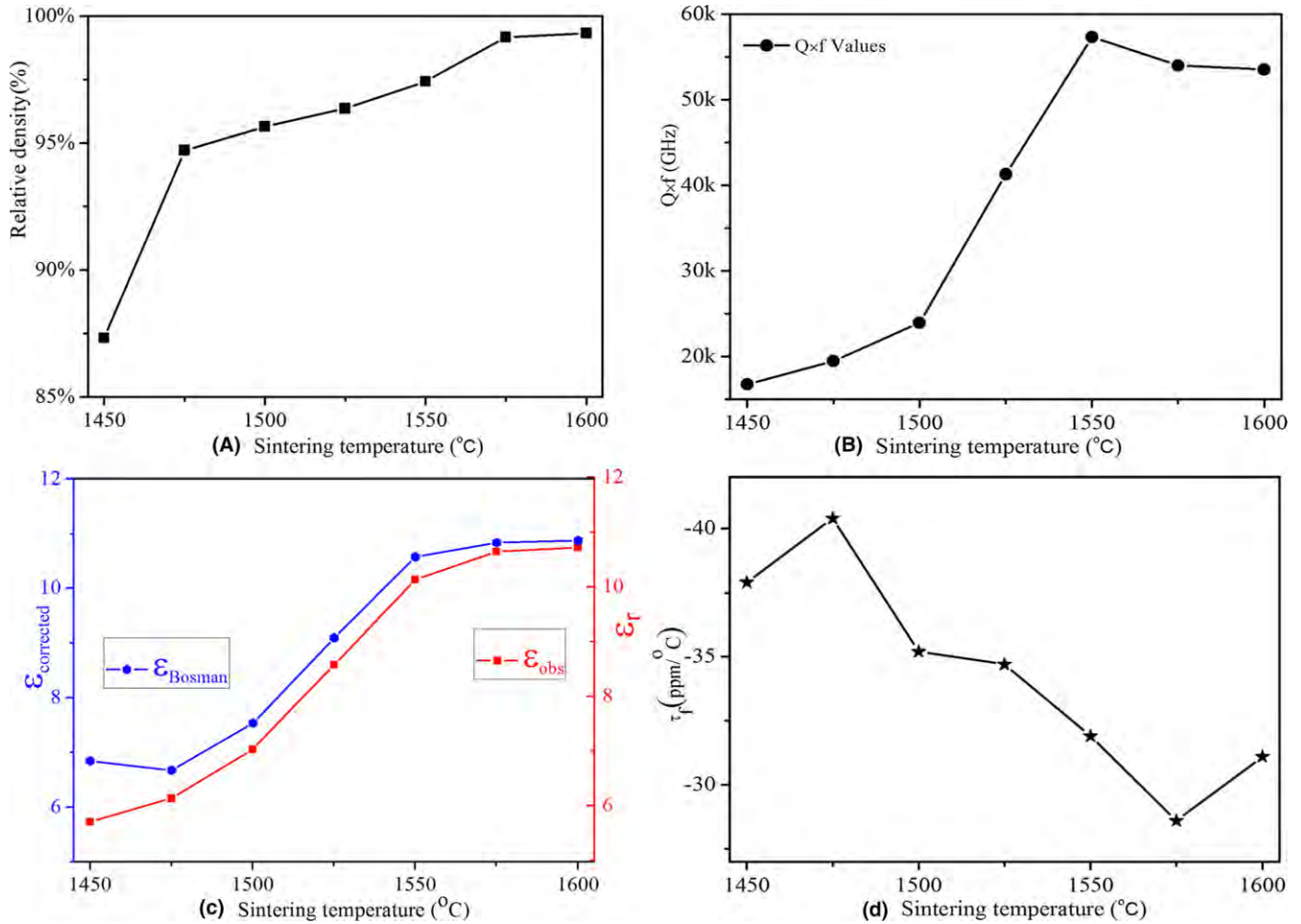
FIGURE 5 The bulk relative densities, quality factors (Qf values), dielectric constants (ε_r), τ_f values of the $Y_3MgAl_3SiO_{12}$ ceramics sintered at different temperature

from internal crystal lattices of grains and finally deteriorate Qf values at higher sintering temperature. For the sample sintered over 1575°C, one of deterioration of quality factors

might be relevant to attributed to oxygen vacancy, besides main factors of nonuniform distribution of grain sizes. Figure 5c presents the dielectric constants (ε_r) change as a

function of sintering temperature. It increases from 5.7 to 10.7 with the sintering temperature increasing from 1450°C to 1600°C. The variation in ε_r presents a similar trend with the relative density, indicating that the porosity acts as the dominating factor of ε_r. The permittivity was corrected by Bosman and Havinga's formula[23] in order to eliminate the influence of porosity:

$$\varepsilon_{Bosman} = \varepsilon_{obs}(1 + 1.5P) \qquad (8)$$

$$P = 1 - \frac{\rho_{mea}}{\rho_{th}} \qquad (9)$$

Where, P is porosity, ε_{Bosman} and ε_{obs} are the corrected and measured dielectric constants, respectively. The corrected value about 10.6 is near to the measured one for $Y_3MgAl_3SiO_{12}$ ceramics sintered at 1550°C, which means that the porosity is negligible to microwave properties of the samples sintered at the densification temperature. Figure 5d displays the change in temperature coefficient of resonant frequency (τ_f) with increasing sintering temperature. It can be seen that the τ_f values vary in the range from -29 to -40 ppm/°C in the sintering temperature from 1450°C to 1600°C. There are $Al(Si)O_4$ tetrahedron, $Al(Mg)O_6$ octahedron and YO_8 dodecahedra in $Y_3MgAl_3SiO_{12}$ crystal structures. It well-known that the orientation and the degree of order of octahedron in perovskite ceramics have critical impact on τ_f value.[24,25] However, how the polyhedrons in $Y_3MgAl_3SiO_{12}$ ceramics affect the temperature coefficient of resonant frequency is further studied in the future. Meanwhile, the τ_f is also necessary to be modified to near zero to meet the requirements of commercial application.[26]

4 | CONCLUSIONS

The garnet structure $Y_3MgAl_3SiO_{12}$ ceramics were prepared by the traditional solid-state sintering reaction method. Rietveld refinement of the powder XRD presents that $Y_3MgAl_3SiO_{12}$ is isostructural to $Y_3Al_5O_{12}$ with cubic crystal system belonged to a space group of Ia-3d. The concrete crystallographic data of atom occupation sites show Mg ions occupy Al_{oct} and Si ions occupy Al_{tet}. The distribution of grain sizes and grain sizes have critical impact on Qf values. The optimal microwave dielectric properties are obtained for $Y_3MgAl_3SiO_{12}$ ceramics sintered at 1550°C for 4 hours with ε_r:10.1, Qf: 57340 GHz), and τ_f: -32 ppm/°C. There might be a potential application as passive devices like dielectric substrates in future microwave communication.

ORCID

Kaixin Song http://orcid.org/0000-0002-4622-1234

REFERENCES

1. Zhang J, Yue ZX, Zhou YY, et al. Microwave dielectric properties and thermally stimulated depolarization currents of $(1-x)$MgTiO_3–xCa$_{0.8}$Sr$_{0.2}$TO_3 ceramics. *J Am Ceram Soc.* 2015;98:1548-1554.

2. Cava RJ. Dielectric materials for applications in microwave communications. *J Mater Chem C.* 2000;11:54-62.

3. Lei S, Fan HQ, Ren XH, et al. Novel sintering and band gap engineering of $ZnTiO_3$ ceramics with excellent microwave dielectric properties. *J Mater Chem C.* 2017;5:4040-4047.

4. Ohsato H, Tsunooka T, Sugiyama T, et al. Forsterite ceramics for millimeterwave dielectrics. *J Electroceram.* 2006;17:445-450.

5. Meng SQ, Yue ZX, Zhuang H, et al. Microwave dielectric properties of $Ba_3(VO_4)_2$–Mg_2SiO_4, composite ceramics. *J Am Ceram Soc.* 2010;93:359-361.

6. Guo YP, Ohsato H, Kakimoto K. Characterization and dielectric behavior of willemite and TiO_2-doped willemite ceramics at millimeter-wave frequency. *J Eur Ceram Soc.* 2006;26:1827-1830.

7. Induja IJ, Sebastian MT. Microwave dielectric properties of mineral sillimanite obtained by conventional and cold sintering process. *J Eur Ceram Soc.* 2017;37:2143-2147.

8. Song KX, Liu P, Su WT, et al. Symmetry of hexagonal ring and microwave dielectric properties of $(Mg_{1-x}Ln_x)_2Al_4Si_5O_{18+x}$ (Ln=La, Sm) cordierite-type ceramics. *J Eur Ceram Soc.* 2015;36:1167-1175.

9. Manu KM, Joseph T, Sebastian MT. Temperature compensated $Sr_2Al_2SiO_7$ ceramic for microwave applications. *J Mater Chem Phys.* 2012;133:21-23.

10. Song KX, Wu S, Liu P, et al. Phase composition and microwave dielectric properties of $SrTiO_3$, modified $Mg_2Al_4Si_5O_{18}$, cordierite ceramics. *J Alloys Compd.* 2015;628:57-62.

11. Zou ZY, Lan XK, Lu WZ, et al. Novel high curie temperature $Ba_2ZnSi_2O_7$ ferroelectrics with low-permittivity microwave dielectric properties. *J Electroceram.* 2016;42:16387-16391.

12. Ji H, Huang Z, Wang L, et al. New garnet structure phosphors, LuYMgAlSiO: Ce (=0–3), developed by solid solution design. *J Mater Chem C.* 2016;4:2359-2366.

13. Papagelis K, Kanellis G, Kourouklis GA, et al. Lattice dynamical properties of the rare earth aluminum garnets ($RE_3Al_5O_{12}$). *J Phy Status Solidi.* 2002;233:134-150.

14. Gorbenko V, Zorenko T, Paprocki K, et al. Epitaxial growth of single crystalline film phosphors based on the Ce3 + doped $Ca_2YMgScSi_3O_{12}$ garnet. *CrystEngComm.* 2017;19:3689-3697.

15. Kotnana G, Jammalamadaka SN. General structure analysis system (GSAS). *J Appl Phys.* 2015;117:562.

16. Hakki BW, Coleman PD. A dielectric resonant method of measuring inductive capacitance in the millimeter range. *IEEE Trans Microw Theory Technol.* 1960;8:402-410.

17. Kajfez D, Gundavajhala A. Measurement of material properties with a tunable resonant cavity. *Electron Lett.* 1993;29:1936-1937.

18. Monteseguro V, Rodríguezhernández P, Muñoz A. Yttrium aluminium garnet under pressure: structural, elastic, and vibrational properties from ab initio studies. *J Alloys Compd*. 2015;118:247-257.

19. Kumar V, Kumari S, Kumar P, et al. Structural analysis by Rietveld method and its correlation with optical properties of nanocrystalline zinc oxide. *Adv Mater Lett*. 2015;6:139-147.

20. Liao Q, Li L, Ren X, et al. New low-loss microwave dielectric material $ZnTiNbTaO_8$. *J Am Ceram Soc*. 2011;94:3237-3240.

21. Ramarao SD, Kiran SR, Murthy VRK. Structural, lattice vibrational, optical and microwave dielectric studies on $Ca_{1-x}Sr_{x-}MoO_4$, ceramics with scheelite structure. *J Mater Res Bull*. 2014;56:71-79.

22. Wang CC, Zhang LW. Surface-layer effect in $CaCu_3Ti_4O_{12}$. *Appl Phys Lett*. 2006;88:323-326.

23. Yoon SH, Kim DW, Cho SY, et al. Investigation of the relations between structure and microwave dielectric properties of divalent metal tungstate compounds. *J Eur Ceram Soc*. 2006;26:2051-2054.

24. Li CC, Wei XY, Yan HX, et al. Microwave dielectric properties of $La_3Ti_2TaO_{11}$, ceramics with perovskite-like layered structure. *J Eur Ceram Soc*. 2012;32:4015-4020.

25. Kim IT, Kim YH, Chung S. Order-disorder transition and microwave dielectric properties of $Ba(Ni_{1/3}Nb_{2/3})O_3$ Ceramics. *Jpn J Appl Phys*. 1995;34:4096-4103.

26. Mirsaneh M, Leisten OP, Zalinska B, et al. Circularly polarized dielectric-loaded antennas: current technology and future challenges. *Adv Funct Mater*. 2008;18:2293-2300.